Received: 18 November 2024 | Revised: 13 February 2025 | Accepted: 4 March 2025

DOI: 10.1002/alz.70136

Alzheimer's & Dementia®
THE JOURNAL OF THE ALZHEIMER'S ASSOCIATION

RESEARCH ARTICLE

Tauopathy after long-term cervical lymphadenectomy

Chenrui Wu[1,2] | **Jiangyuan Yuan**[1] | **Yu Tian**[1] | **Youlin Wang**[3] | **Xianghui He**[3] | **Ke Zhao**[3] | **Jinhao Huang**[1] | **Rongcai Jiang**[1,4]

[1]Department of Neurosurgery, Tianjin Neurological Institute, State Key Laboratory of Experimental Hematology, Laboratory of Post-Neuroinjury Neurorepair and Regeneration in Central Nervous System Tianjin & Ministry of Education, Tianjin Medical University General Hospital, Tianjin, China

[2]Department of Neurosurgery, Sichuan Provincial People's Hospital, University of Electronic Science and Technology of China, Chengdu, China

[3]Department of General Surgery, Tianjin Medical University General Hospital, Tianjin, China

[4]Department of Neurosurgery, Xuanwu Hospital, Capital Medical University, Beijing, China

Correspondence
Jinhao Huang, Department of Neurosurgery, Tianjin Neurological Institute, State Key Laboratory of Experimental Hematology, Laboratory of Post-Neuroinjury Neurorepair and Regeneration in Central Nervous System Tianjin & Ministry of Education, Tianjin Medical University General Hospital, No. 154, Anshan Road, Heping District, Tianjin, China.
Email: Jinhao.huang@tmu.edu.cn

Rongcai Jiang, Department of Neurosurgery, Xuanwu Hospital, Capital Medical University, No. 45 Changchun Street, Xicheng District, Beijing, China.
Email: jiangrongcai@tmu.edu.cn

Funding information
National Natural Science Foundation of China, Grant/Award Numbers: 82071390, 82271394, 82071402, 82171359, 82001323, 82101434; Tianjin Key Medical Discipline (Specialty) Construction Project

Abstract

INTRODUCTION: This study examined the effects of long-term cervical lymphadenectomy (cLE) on cognitive and Alzheimer's disease (AD)–like tauopathy changes.

METHODS: Male C57BL/6 mice were used to assess cLE impacts on sleep, brain pathways, and pathologies. RNA sequencing and proteomics analyzed gene/protein changes, with results verified by western blotting and immunofluorescence.

RESULTS: CLE led to sleep and psychiatric disorders, linked to mitogen-activated protein kinase/extracellular signal-regulated kinase (ERK) pathway activation. Activation of ERK may interfere with autophagy and is associated with phosphorylated tau accumulation. Peripheral blood analysis shows decreased brain waste in the peripheral blood post-cLE, implicating impaired lymphatic drainage and brain waste build-up.

DISCUSSION: These findings suggest a potential connection between cLE and AD-like tauopathy, potentially influencing surgical decisions.

KEYWORDS
Alzheimer's disease, brain lymphatic system, cervical lymph nodes, neurofibrillary tangles, phosphorylated tau

Highlights

- Cervical lymphadenectomy (cLE) is the cornerstone of head and neck cancers, affecting millions of people each year. We provide the first evidence of mildly impaired cognitive functioning with significant anxiety–depressive disorders in mice after long-term cLE.
- Long-term cLE not only directly impairs brain wastes (amyloid beta, phosphorylated tau [p-tau]) drainage, but also activates the Erk1/2 signaling pathway leading to attenuation of autophagy.

Chenrui Wu, Jiangyuan Yuan, and Jinhao Huang contributed equally to this work.

- We found for the first time that long-term cLE accelerated the deposition of p-tau in young mice.
- Patients after clinical cervical lymph node dissection showed reduced brain waste in peripheral blood consistent with mouse models. This study suggests the need for further evaluation of the neurologic effects of cervical lymph node dissection, a procedure that affects millions of people each year.

1 | BACKGROUND

Cervical lymphadenectomy (cLE), a surgical procedure commonly performed to treat malignancies of the oral cavity, pharynx, esophagus, and thyroid gland, involves the removal of lymph nodes in the cervical region.[1–3] This procedure is a cornerstone in managing these cancers, with millions of individuals worldwide undergoing cLE annually.[4] While the primary focus of this surgery has traditionally been the effective treatment of cancer, the potential long-term consequences that extend beyond oncological outcomes, particularly concerning neurological health, have not been studied.

Alzheimer's disease (AD) is a progressive neurodegenerative disorder marked by cognitive decline, memory loss, and behavioral changes.[5] In addition to these primary symptoms, mental disorders such as anxiety and depression,[6,7] as well as sleep disturbances,[8,9] are essential preexisting conditions and independent risk factors in patients with AD. These non-cognitive symptoms not only intensify the overall disease burden but also significantly diminish the quality of life for both affected individuals and their caregivers. Interestingly, similar mental and sleep disturbances have been observed in patients with head and neck cancers. Clinical studies indicate that patients with head and neck cancer have a higher incidence of depression compared to those with other types of cancer.[10,11] Notably, patients who underwent only surgical treatment showed more severe depression scores than those who received only radiation therapy.[12]

Furthermore, patients who underwent cLE reported poorer sleep quality than those who did not undergo this procedure.[13] This evidence suggests that the surgical removal of cervical lymph nodes may contribute to the onset or worsening of mental and sleep disorders in this patient population. This overlap raises intriguing questions about the potential link between cLE and the development or exacerbation of AD-like pathology.

The cervical lymph nodes play a critical role in draining cerebrospinal fluid and interstitial fluid from the brain through the meningeal lymphatic and glymphatic system.[14,15] These systems are essential components of the brain's waste clearance mechanism, facilitating the removal of brain wastes, including amyloid beta (Aβ) peptides and phosphorylated tau (p-tau) protein, which are implicated in the pathogenesis of AD.[16,17] Disruption of these pathways, such as through the removal of cervical lymph nodes, could theoretically impair the brain's ability to clear these toxic substances, potentially accelerating neurodegenerative processes.

In animal models of AD, it has been well documented that impairing the meningeal lymphatic system or cervical lymph nodes exacerbates disease progression. Da Mesquita et al. found that meningeal lymphatic dysfunction may be an aggravating factor in AD pathology and age-related cognitive decline.[16,18] Similar results were observed in AD mice with cLE intervention.[19,20] These findings suggest that the lymphatic system plays a significant role in modulating neurodegenerative processes and raise concerns about the possible long-term neurological effects of cLE.

Despite the increasing recognition of the meningeal lymphatic system's importance in neurological health, the long-term effects of cLE on brain function in normal, non-transgenic animals have not been thoroughly investigated. This knowledge gap is particularly concerning given the widespread use of cLE and its potential to affect millions of patients worldwide. The possibility that this standard surgical procedure could predispose individuals to AD-like pathology necessitates further investigation.

This study aims to investigate the potential long-term consequences of cLE on the brain, focusing on the development of AD-like pathology. Additionally, the study seeks to elucidate the underlying molecular pathological mechanisms using a comprehensive multi-omics approach. By examining the effects of cLE in animal models, this research aims to provide critical insights that could influence surgical decision making and postoperative care in patients undergoing this procedure. Understanding these effects is crucial for developing strategies to mitigate any adverse outcomes and ensure that the benefits of cLE are not overshadowed by unforeseen neurological risks.

2 | METHODS

2.1 | Animal surgery and tissue acquisition

This study was approved by the animal welfare ethics committee of Tianjin Medical University General Hospital (Approval number: IRB2024-DW-79). Male C57BL/6 mice aged 4 to 6 weeks were used for all experiments. The animals were housed under standard laboratory conditions (12 hour light/dark cycle, temperature 22°C ± 2°C, and ad libitum access to food and water).

Mice in the cLE group underwent bilateral deep and superficial cervical lymphadenectomy (mandibular lymph node, accessory mandibular lymph node, superficial parotid lymph node, and caudal

deep cervical lymph node)[21,22] using a micro electrocoagulator. The mice in the sham-operated group underwent bilateral cervical lymph node exploration, but no removal was performed. All surgical procedures were performed under gas anesthesia with isoflurane (2% for induction, 1%–1.5% for maintenance) to minimize pain and discomfort. The anesthetic time for the sham group was 30 minutes, while for the cLE group, due to the operation, the anesthetic time ranged from 20 to 30 minutes. Postoperative analgesia was provided via subcutaneous injection of carprofen (5 mg/kg) every 24 hours for 48 hours. Six months post-surgery, behavioral tests were conducted, and tissues were harvested after deep anesthesia euthanasia (6% isoflurane) for subsequent analyses. All mice underwent perfusion with 30 mL of 4°C phosphate-buffered saline (PBS) before brain tissue was collected.

2.2 | Behavioral tests

Behavioral assessments were conducted to evaluate cognitive and anxiety-related behaviors 6 months post-surgery. The following tests were performed using the EthoVision XT system (Noldus) for data acquisition and analysis. In the open field and elevated plus-maze tests, the area was cleaned with 75% ethanol between trials for the two mice, followed by cleaning with water and drying with paper towels.

The Morris water maze (MWM) test included a hidden platform trial for spatial learning and a probe trial for memory retention. Each trial was conducted in a circular pool (diameter: 100 cm), with water made opaque using non-toxic white paint. Mice underwent four trials per day for 5 consecutive days. The probe trial was performed in two quadrants, and the results were averaged. The escape latency to the hidden platform was recorded.

For the open field test (OFT), mice were placed in the center of an open field arena (40 cm × 40 cm) for 10 minutes to assess locomotor activity and anxiety-like behavior. The total distance traveled and time spent in the center versus the periphery of the arena were measured.

The elevated plus-maze test (EPT) assessed anxiety-related behavior. Mice were placed in the center of a plus-shaped apparatus elevated 50 cm above the floor, with two open arms and two closed arms. The time spent in open versus closed arms over a 5 minute session was recorded.

The tail suspension test (TST) evaluated depressive-like behavior. Mice were suspended by their tails for 6 minutes, and immobility time was recorded as an indicator of despair-like behavior.

2.3 | Brain tissue bulk RNA sequencing and analysis

Mice were euthanized under deep anesthesia (6% isoflurane). After perfusion of 30 mL of 4°C PBS, the brain was rapidly dissected on ice and the meninges, olfactory bulb, and cerebellum were removed (6 mice per group). Gene Denovo Biotechnology, a company providing commercial services, conducted RNA sequencing (RNA-seq) and analyzed the data in Guangzhou, China. Cerebrum tissues were collected and snap-frozen in liquid nitrogen. Total RNA was extracted using the TRIzol reagent, and RNA quality was assessed using an Agilent Bioanalyzer. Libraries were prepared using the Stranded mRNA Prep Kit (Illumina, 20040534), and sequencing was performed on an Illumina NovaSeq 6000 platform. In our study, genes with < 1 count per million (CPM) in at least 50% of the samples were excluded by the edgeR package. Differential expression analysis was conducted using DESeq2 package,[23] with significant genes defined as those with an unadjusted p value < 0.01. The clusterProfiler package was used to perform functional pathway enrichment analyses.

RESEARCH IN CONTEXT

1. **Systematic review**: The authors reviewed literature from PubMed and Google Scholar. The brain lymphatic system plays a crucial role in waste clearance. Cervical lymph nodes are essential drainage points, but their dissection's impact on brain waste clearance and Alzheimer's disease (AD) remains unclear.
2. **Interpretation**: Our evidence shows long-term sleep and psychiatric disorders post-cervical lymphadenectomy (cLE) with mitogen-activated protein kinase/extracellular signal-regulated kinase pathway activation, which inhibits autophagy, leading to phosphorylated tau accumulation. The study also shows decreased brain waste levels in peripheral blood post-cLE, indicating impaired drainage and accumulation of brain waste.
3. **Future directions**: Our findings suggest a potential link between cLE and AD-like pathology, which may have significant implications for surgical decision making in millions of patients.

2.4 | Brain tissue proteomics and analysis

Frozen samples were ground in liquid nitrogen, homogenized in 1 mL phenol extraction buffer, and 1 mL Tris-HCl (pH 7.5) saturated phenol was added. The mixture was shaken, kept at 4°C for 30 minutes, and centrifuged at 7100 g for 10 minutes. The phenolic phase was mixed with five volumes of 0.1 M ammonium acetate-methanol, kept at −20°C overnight, and centrifuged at 12,000 g for 10 minutes. The pellet was washed with methanol and acetone, air dried, and resuspended in 300 µL lysate solution. It was then incubated 3 hours at room temperature, centrifuged, and supernatant was quantified via bicinchoninic acid assay. Equal protein amounts were diluted to the same concentration and volume. Twenty-five mM dithiothreitol was added to make the final 5 mM, incubated at 55°C for 30 to 60 minutes, then Iodoacetamide was added (10 mM) and incubated for 15 to 30 minutes at room temperature. Precipitate with six volumes of acetone was kept at −20°C for 4 hours, then centrifuged at 8000 g for

10 minutes at 4°C. The pellet was redissolved in enzymolysis diluent (protein:enzyme = 50:1), incubated at 37°C for 12 hours, then lyophilized or evaporated post-enzymolysis.

For tandem mass tag (TMT) labeling, lyophilized samples were resuspended in 30 µL 100 mM tetraethylammonium bromide. A total of 20 µL acetonitrile was added to the TMT reagent, dissolved for 5 minutes, mixed, and centrifuged twice. A total of 10 µL TMT label reagent was added per sample, mixed, and incubated for 1 hour. A total of 5 µL 5% hydroxylamine was added and incubated for 15 minutes. Samples were lyophilized and stored at −80°C.

Using immobilized metal ion affinity chromatography (IMAC), peptides were suspended in 200 µL buffer, equilibrated columns were balanced, peptides were added, incubated for 30 minutes, centrifuged at 1000 g for 30 seconds, placed in new tubes, elution buffer was added, and then centrifuged at 1000 g for 30 seconds twice. Elution buffer was dried in a vacuum concentrator.

Proteomic analysis was performed by Shanghai Luming (Shanghai, China) using Q Exactive HF mass spectrometer (Thermo Fisher), then loaded by Acclaim PepMap RSLC on EASY-nLCTM 1200 system. Flow rate was 300 nL/minute at gradient: 0 to 40 minutes, 5% to −30% B; 40 to 55 minutes, 30% to 50% B; 55 to 60 minutes, 50% to 100% B. Full mass spectrometry (MS) scans were done at 300 to 1600 m/z, 70,000 resolution, automatic gain control (AGC) target 1e6. Most intense peaks were fragmented by higher-energy collision dissociation (HCD, energy 28).

Tandem mass spectrometry (MS/MS) spectra were at 35,000 resolution, AGC target 2e5, max injection time 80 ms, dynamic exclusion 15 seconds, positive mode. MS/MS spectra were searched with MaxQuant against Uniprot Mus Musculus. The fixed modifications applied were Carbamidomethylation on cysteine (C) and TMT labeling on the N-terminus and lysine (K). The variable modifications included phosphorylation on serine, threonine, and tyrosine (phospho on STY), oxidation on methionine (oxidation on M), and acetylation on the protein N-terminus (acetyl on Protein N-term). Trypsin was used for digestion. The peptide tolerance was set at 20 ppm for the first search and 4.5 ppm for the main search. Additionally, the maximum number of missed cleavages allowed was 2.

Proteins/phosphopeptides were identified by p value < 0.05. Phosphorylation motifs were analyzed with MoMo,[24] and protein annotations via Gene Ontology (GO) and Kyoto Encyclopedia of Genes and Genomes (KEGG). GO and KEGG enrichment analyses were performed on differentially expressed proteins/phosphopeptides.

2.5 | Protein extraction and western blotting

For protein analysis, brain tissues were homogenized in radioimmunoprecipitation assay buffer (50 mM Tris-HCl, pH 7.4, 150 mM NaCl, 1% NP-40, 0.5% sodium deoxycholate, 0.1% sodium dodecyl sulfate [SDS]) supplemented with protease inhibitors (Roche, 05892970001) and phosphatase inhibitors (Thermo Fisher Scientific, A32957). Protein concentration was determined using the BCA Protein Assay Kit (Thermo Fisher Scientific, 23225). Equal amounts of protein (50 µg) were separated by SDS polyacrylamide gel electrophoresis and transferred to 0.45 µm polyvinylidene fluoride (PVDF) membranes (Millipore, IPVH00005) or 0.2 µm PVDF membranes (Millipore, ISEQ00005). Membranes were blocked with 5% non-fat dry milk in TBST and probed with primary antibodies overnight at 4°C. After a 1 hour incubation of the PVDF membrane with the horseradish peroxidase–conjugated secondary antibody (1:5000, Thermo Fisher Scientific, 32460, A16066), the membrane was developed using the enhanced chemiluminescent reagent (Millipore, WBULP-100ML) and subsequently photographed. The bands were quantified using ImageJ software.

2.6 | Brain tissue frozen section and immunofluorescence double labeling co-localization

Brains were fixed in 4% paraformaldehyde at 4°C overnight, cryoprotected in 30% sucrose, and embedded in the optimal cutting temperature compound. Frozen sections (10 µm thick) were cut using a cryostat and mounted on glass slides. Sections were permeabilized with 0.3% Triton X-100, blocked with 5% normal goat serum, and incubated with primary antibodies overnight at 4°C. Secondary antibodies conjugated to Alexa 488 or 594 Fluor dyes (Thermo Fisher Scientific, A-11008, A-11005) were used for detection. Slides were mounted with a DAPI-containing mounting medium and visualized using a fluorescence microscope (Olympus, IX73). We used ImageJ software to binarize the NeuN channel images and counted the total number of NeuN-positive cells. The binarized NeuN images were then used as a mask for the Proopiomelanocortin (POMC) channel images to count the number of POMC-positive NeuN cells.

2.7 | Primary antibodies

Primary antibodies used include: Per2 Rabbit pAb (Abclonal, A13168, 1:1000 for Western Blotting); Npas2 Rabbit pAb (Abclonal, A16930, 1:1000 for western blotting); Pomc Rabbit pAb (Abclonal, A3038, 1:1000 for western blotting, 1:100 for immunofluorescence); NeuN mouse mAb (Millipore, MAB377, 1:200 for immunofluorescence); p-MEK1/2 Rabbit mAb (Cell Signaling Technology, #2338, 1:2000 for western blotting); p-Erk1/2 Rabbit mAb (Cell Signaling Technology, #4370, 1:2000 for western blotting); t-Erk1/2 Rabbit pAb (Cell Signaling Technology, #9102, 1:1000 for western blotting); p-p38 Rabbit mAb (Cell Signaling Technology, #4511, 1:1000 for western blotting); LC3B Rabbit mAb (Cell Signaling Technology, #3868, 1:1000 for western blotting); Atg12 Rabbit mAb (Abclonal, A22788, 1:500 for western blotting); Beclin1 Rabbit mAb (Abclonal, A21191, 1:5000 for western blotting); p62 Rabbit mAb (Abclonal, A19700, 1:20000 for western blotting); Ki67 Rabbit mAb (Abcam, ab16667, 1:1000 for western blotting, 1:200 for immunofluorescence); APP Rabbit mAb (Abcam, ab32136, 1:10000 for western blotting); Aβ1-42 Rabbit mAb (Abcam, ab201060, 1:5000 for western blotting); p-tau205 Rabbit mAb (Abclonal, AP1445, 1:500 for western blotting, 1:100

for immunofluorescence); p-tau217 Rabbit mAb (Abclonal, AP1373, 1:5000 for western blotting); p-tau262 Rabbit pAb (Abclonal, AP0397, 1:200 for western blotting); p-tau396 Rabbit mAb (Abclonal, AP1028, 1:1000 for western blotting); p-tau404 Rabbit mAb (Abclonal, AP1378, 1:2000 for western blotting).

2.8 | Mouse cortical electroencephalogram monitoring

Electroencephalogram (EEG) monitoring was performed with reference to our previous steps.[25] In brief, mice were induced to sleep by gavage of 5% chloral hydrate (Macklin, C804539, 0.5 mL/20 g) prior to performing EEG (Natus Medical). EEG was performed 6 months after cLE. One active electrode was implanted under the scalp in the middle of the skull, and two reference electrodes were implanted at the mastoid process. The sleep EEG of each mouse was recorded in a dark environment for at least 10 minutes until they resumed motor activity. The energy spectral density of each EEG wave (alpha, beta, theta, and delta) was analyzed by the EEG viewer (Natus Medical).

2.9 | Enzyme-linked immunosorbent assay detection of plasma Aβ and p-tau396 levels

Blood samples were collected from mice via retro-orbital bleeding, and human samples were collected from peripheral veins. The samples were placed into ethylenediaminetetraacetic acid-coated tubes and centrifuged at 2000 × g for 10 minutes at 4°C to obtain plasma. Plasma levels of Aβ and p-tau396 were measured using specific enzyme-linked immunosorbent assay kits (Aβ1-42 and p-tau, Elabscience, E-EL-M3010, E-EL-H0543, E-EL-M1289, E-EL-H5314) according to the manufacturer's instructions. Absorbance was read at 450 nm using a microplate reader (BioTek, SYNERGY2).

2.10 | Transmission electron microscopy

Transmission electron microscopy (TEM) experiments were performed as detailed previously.[25] Briefly, 1 mm^3 cortex tissues were fixed in 4% glutaraldehyde for 48 hours, followed by immersion in 1% osmium tetroxide solution for 1 hour. After dehydration in ethanol, the samples were sectioned into 70 nm-thick slices, which were then placed on grids. The grids were stained with uranyl acetate and lead citrate before being examined under a transmission electron microscope (HT7800, Hitachi, Japan).

2.11 | Clinical patient enrollment and data collection

The clinical ethics committee of the Tianjin Medical University General Hospital approved the clinical trials in this study (approval number: IRB2024-YX-429-01). This observational clinical study was registered at the Chinese Clinical Trial Registry (ChiCTR). Patients were included between April 2023 and April 2024 at the General Hospital of Tianjin Medical University. Inclusion criteria were: (1) diagnosed with thyroid cancer and prepared for thyroidectomy and bilateral cervical lymph node dissection (central neck dissection); (2) aged 16 to 70 years; (3) had not undergone head and neck surgeries or suffered from head and neck trauma; (4) did not suffer from sleep disorders, psychiatric disorders, and neurodegenerative disorders; and (5) signed an informed consent form. Exclusion criteria were: (1) postoperative infection, bleeding, nerve injury, poor healing, unplanned secondary surgery; (2) insufficient intraoperative lymph node dissection; (3) undergoing other head and neck surgery or suffering head and neck trauma after the surgery; (4) brain metastasis detected during hospitalization or follow-up; (5) pregnancy during postoperative follow-up. Blood samples were collected from patients 1 day before surgery, 3 days after surgery, and 6 months after surgery. Plasma was isolated as described above and stored at −80°C until analysis. Sleep and psychiatric scores were assessed 1 day before and 6 months after surgery. Sleep quality was assessed using the Pittsburgh Sleep Quality Index (PSQI), and anxiety and depression were assessed using the Hospital Anxiety and Depression Scale (HADS).

2.12 | Statistical analysis

Statistical analyses were conducted using GraphPad Prism software (version 9.0). Normality tests were performed. Two independent samples were analyzed using a two-tailed *t* test, while datasets were examined with one-way or two-way analysis of variance, followed by the Tukey post hoc test. Pre- and post-surgery data for the same clinical patients were analyzed using a two-tailed paired *t* test. Multifactor correlation analysis and visualization were performed using the Spearman algorithm in the corrplot package of R language. A p value of < 0.05 was considered statistically significant. All data are presented as mean ± standard deviation.

3 | RESULTS

3.1 | Cognitive dysfunction and mental disorders after long-term cLE

Cognitive dysfunction is a primary symptom of AD. To assess the impact of long-term cLE on cognitive function, we conducted the MWM test on cLE and sham-operated mice to evaluate their learning and memory capabilities ($n = 10$ mice per group). Both groups underwent hidden platform training from day 1 to 5 (Figure S1A in supporting information), followed by a probe trial on day 6 (Figure S1B). Throughout the training period, no significant differences were observed in escape latencies between the sham and cLE groups (Figure S1A, day 1–5: $p > 0.05$). Similarly, during the probe trial on day 6, there were no significant differences between the groups regarding the platform crossover

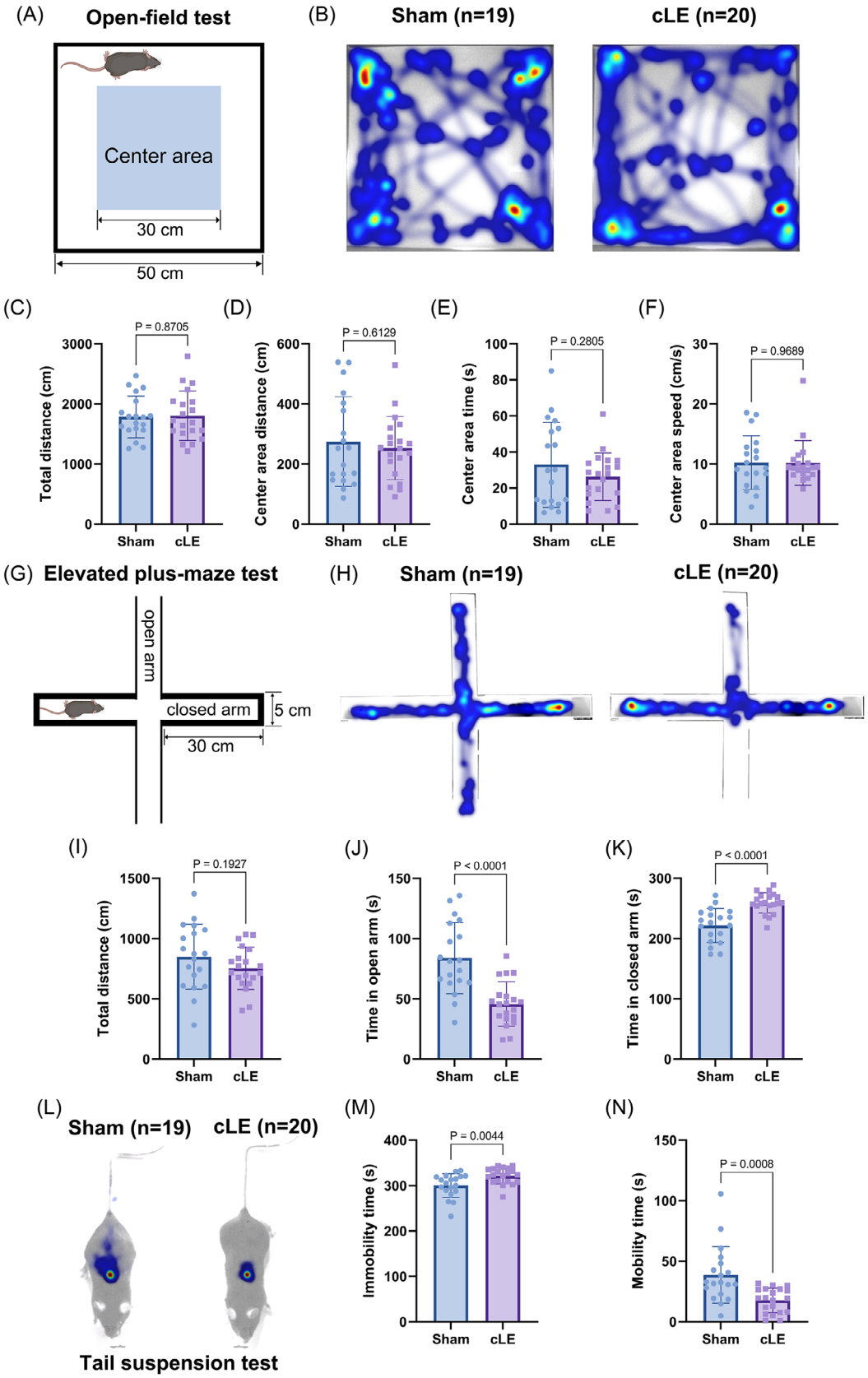

FIGURE 1 Long-term cervical lymphadenectomy (cLE) induces depression-like behavior. A, Schematic diagram of the open-field test (OFT) area. Mice are placed in a 50 cm square closed space with the central area defined as a 30 cm square. B, Representative heat maps of OFT trajectories for sham and cLE group mice (sham group $n = 19$; cLE group $n = 20$). C, Total distance moved by mice in the OFT ($p = 0.8705$). D, Distance moved in the central area in the OFT ($p = 0.6129$). E, Time spent in the central area in the OFT ($p = 0.2805$). F, Speed of movement in the

number, escape latency, and swimming speed (Figure S1B, $p > 0.05$). However, the sham group spent more time in the platform quadrant than the cLE group (Figure S1B, $p = 0.0180$).

Given the almost negative results from the MWM test, we sought to investigate potential early mental signs of AD in another batch of mice (sham group, $n = 19$; cLE group, $n = 18$). We performed the OFT in a 50 cm square enclosed space (Figure 1A,B). The OFT results indicated no significant differences in the total distance traveled between the two groups ($p = 0.8705$, Figure 1C). Although the cLE group exhibited lower mean values for center area distance and time than the sham group, these differences were not statistically significant (center area distance: $p = 0.6129$, Figure 1D; center area time: $p = 0.2805$, Figure 1E). Additionally, both groups had similar speeds in the center area ($p = 0.9689$, Figure 1F).

Interestingly, significant psycho-behavioral differences between the two groups emerged in the EPT and the TST. The EPT was conducted using an apparatus elevated 1.5 m above the ground, featuring open and closed arms, each 30 cm long and 5 cm wide (Figure 1G). Heat maps of activity areas revealed a significant reduction in the frequency of activity in the open arm for the cLE group (Figure 1H). Although there was a slight decrease in the total distance traveled by the cLE group, this was not statistically significant ($p = 0.1927$, Figure 1I). However, the cLE group spent significantly less time in the open arm ($p < 0.0001$, Figure 1J) and more time in the closed arm ($p < 0.0001$, Figure 1K). Similarly, in the TST (Figure 1L), the cLE group displayed significantly more extended periods of inactivity compared to the sham group ($p = 0.0044$, Figure 1M) and shorter periods of activity ($p = 0.0008$, Figure 1N). These results support the occurrence of depression-like behavior after long-term cLE.

3.2 | Sleep disorders after long-term cLE

To further investigate the molecular pathological mechanisms underlying depression-like behavior after long-term cLE, we conducted bulk RNA-seq of mice brains in the sham group ($n = 6$) and the cLE group ($n = 6$). The RNA-seq results revealed that 6 months post-cLE, 98 genes were upregulated ($p < 0.01$, log2Foldchange > 0), 96 genes were downregulated ($p < 0.01$, log2Foldchange < 0), and 22,079 genes showed no significant differential expression ($p > 0.01$, Figure 2A). From these 194 differentially expressed genes, we identified eight overlapping genes (*Pomc*, *Dusp1*, *Npas2*, *Mmab*, *Map2k5*, *Atp2a2*, *Per3*, and *Per2*; Figure 2B) by intersecting them with the top 300 genes associated with depressive disorder (C0011581) from the DisGeNET database.[26] The $\log_2$Foldchange of these eight genes is depicted in Figure 2C, with *Pomc* exhibiting the most significant downregulation (cLE vs. sham, Figure 2C). KEGG functional enrichment analysis indicated that these genes predominantly involve circadian rhythm, particularly *Npas2*, *Per2*, and *Per3* (highlighted in red in Figure 2C,D). POMC is a precursor polypeptide that plays a crucial role in regulating various physiological processes, including circadian rhythms and responses to photoperiods.[27] To further elucidate changes at the protein level, we conducted western blotting (Figure 2E). The results demonstrated an upregulation of *Per2* and a significant downregulation of *Pomc* in the brain post-cLE, with no notable change in *Npas2* expression (*Per2*: $p = 0.0135$; *Npas2*: $p = 0.2303$; *Pomc*: $p < 0.0001$; Figure 2F-H). *Pomc* levels were significantly decreased in neurons of the hippocampal CA1 region, hippocampal dentate gyrus (DG) region, and thalamus, while no significant changes were observed in cortical neurons, as revealed by immunofluorescence co-localization (Figure 2I,J, Figure S2 in supporting information). To objectively assess the sleep quality of the mice, we performed a quantitative EEG analysis (Figure 2L). The EEG data showed a significant increase in α and θ waves and a significant decrease in δ waves in cLE mice, suggesting that cLE leads to increased light sleep (non–rapid eye movement [NREM] stage 1 and NREM stage 2) and reduced deep sleep (NREM stage 3;[28] α: $p = 0.0061$; β: $p = 0.2310$; θ: $P = 0.0043$; δ: $p = 0.0041$; Figure 2M).

Based on the above results, we speculate that cLE disrupts the expression of circadian rhythm–related proteins and is associated with increased light sleep and decreased deep sleep, which may exacerbate the risk of depression-like behaviors (Figure 2N).

3.3 | Disturbed autophagy after long-term cLE with mitogen-activated protein kinase/extracellular signal-regulated kinase pathway activation

Proteins are the primary executors of cellular functions. To investigate the molecular consequences of long-term cLE, we used quantitative proteomics and phosphoproteomics in sham ($n = 4$) and cLE ($n = 4$) groups. Proteomics analysis revealed that 125 proteins were upregulated ($p < 0.05$, log2Foldchange > 0), 400 were downregulated ($p < 0.05$, log2Foldchange < 0), and 6635 showed no significant change ($p > 0.05$, Figure 3A). KEGG pathway enrichment of these differentially expressed proteins primarily implicated autophagy-related function (highlighted in red, Figure 3B). Chord diagram analysis further identified differentially expressed autophagy-related proteins, including ATG12, ATG4C, ATG3, MLST8, ATG5, BNIP3, RAB33B, MAP1LC3A, DAPK3, and EPG5 (marked in red, Figure 3C). Phosphoproteomics of the same samples showed 156 phosphorylation sites with increased

central area in the OFT ($p = 0.9689$). G, Schematic diagram of the elevated plus-maze test (EPT) apparatus. Both the closed and open arms are 30 cm long and 5 cm wide, with the closed arms enclosed by 40 cm high walls. The entire maze is elevated 1 m above the ground. H, Representative heat maps of EPT trajectories for sham and cLE group mice (sham group $n = 19$; cLE group $n = 20$). I, Total distance moved by mice in EPT ($p = 0.1927$). J, Time spent in the open arms in EPT ($p < 0.0001$). K, Time spent in the closed arms in EPT ($p < 0.0001$). L, Representative heat maps of the center body-point trajectories in the tail suspension test (TST) for sham and cLE group mice (sham group $n = 19$; cLE group $n = 20$). M, Duration of immobility in TST ($p = 0.0044$). N, Duration of activity in TST ($p = 0.0008$).

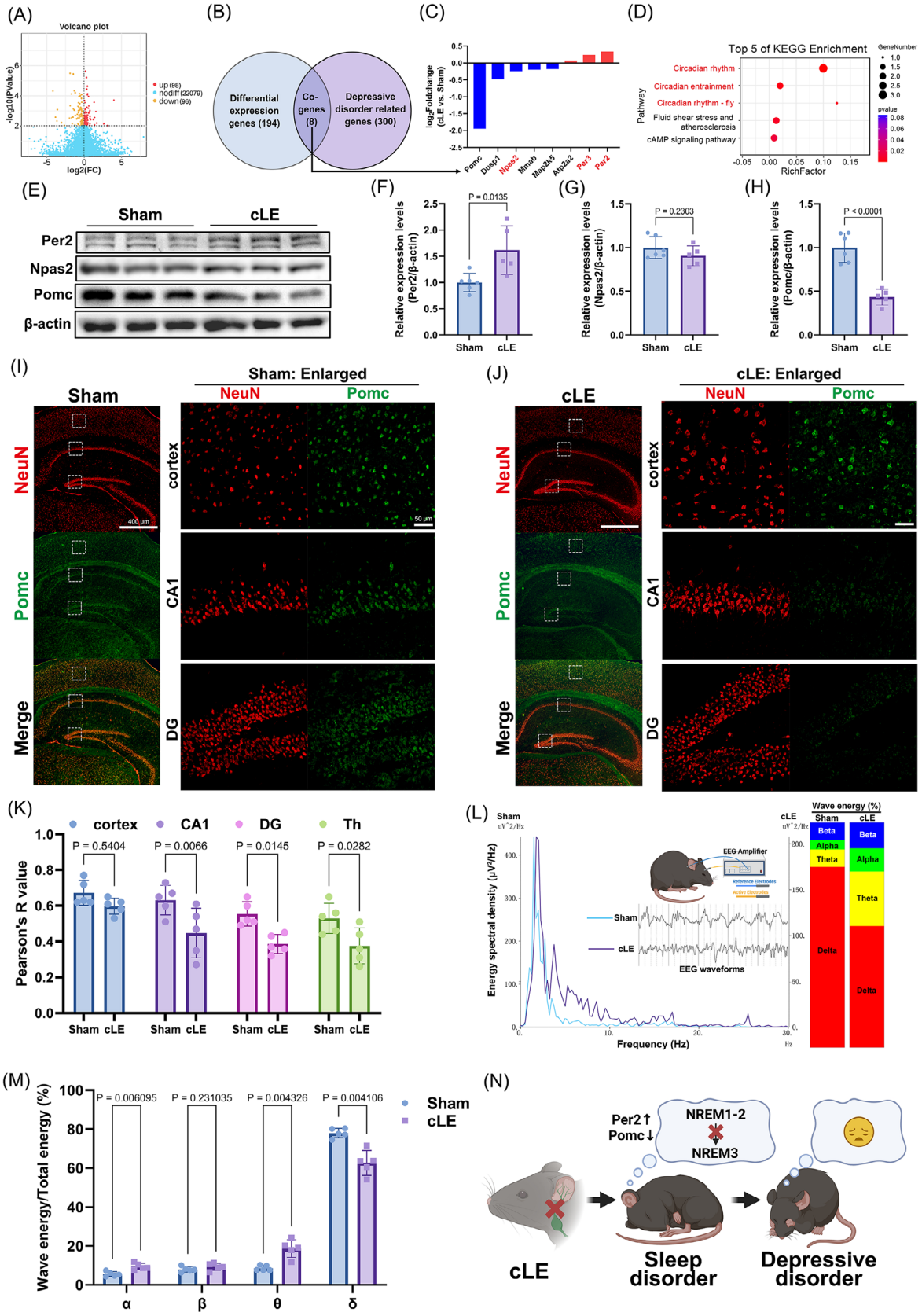

FIGURE 2 Long-term cervical lymphadenectomy (cLE) leads to sleep disorders. A, The volcano plot illustrates the number of upregulated and downregulated differentially expressed genes in brain tissue bulk RNA sequencing results after cLE ($p < 0.01$, $n = 6$ mice per group). B, Intersection of all differentially expressed genes with depressive disorder-related genes identifying eight overlapping genes. C, Differential expression levels of the eight overlapping genes: *Pomc*, *Dusp1*, *Npas2*, *Mmab*, *Map2k5*, *Atp2a2*, *Per3*, and *Per2*. D, Kyoto Encyclopedia of Genes and Genomes (KEGG)

phosphorylation levels ($p < 0.05$, log2Foldchange > 0), 179 with decreased phosphorylation levels ($p < 0.05$, log2Foldchange < 0), and 5512 without significant changes ($p > 0.05$, Figure 3D). KEGG enrichment analysis suggested that, in addition to autophagy, the differentially phosphorylated proteins are closely associated with upstream pathways regulating autophagy, including the mitogen-activated protein kinase (MAPK), mechanistic target of rapamycin (mTOR), and PI3K signaling pathways (highlighted in red, Figure 3E). Based on these findings, we hypothesize that MAPK/extracellular signal-regulated kinase (ERK) pathway activation after long-term cLE inhibits autophagy (Figure 3F). To validate these proteomics results, we assessed MAPK and mTOR pathway phosphorylation levels via western blotting (Figure 3G). The results indicated a significant increase in MEK1/2 phosphorylation in the cLE group (p-MEK1/2/t-MEK1/2: $p = 0.0040$; p-MEK1/2/β-actin: $p = 0.0011$; Figure 3H,I), along with a significant increase in Erk1/2 phosphorylation (p-Erk1/2/t-Erk1/2: $p = 0.0188$; p-Erk1/2/β-actin: $p = 0.0114$; Figure 3J,K). Meanwhile, mTOR phosphorylation was enhanced in the cLE group (p-mTOR/t-mTOR: $p = 0.0029$; p-mTOR/β-actin: $p = 0.0009$; Figure 3L,M). Although p38, another MAPK family member, showed increased phosphorylation after cLE, the change was insignificant ($p = 0.1473$, Figure 3N). Additionally, we examined the expression levels of autophagy-related proteins (Figure 3O). The results revealed a decrease in the LC3B-II/LC3B-I ratio ($p = 0.0345$, Figure 3P) and reductions in Atg12 ($p = 0.0054$, Figure 3Q) and Beclin-1 ($p = 0.0019$, Figure 3R) protein levels, while p62 levels remained unchanged ($p = 0.2513$, Figure 3S).

Through integrated multi-omics analysis, supported by western blot validation, we concluded that autophagy is disturbed in the brain after long-term cLE, potentially due to ERK and mTOR pathway activation.

3.4 | Long-term cLE does not affect thyroid cell proliferation and reduces MAPK pathway phosphorylation

Neck lymph node dissection is a prevalent surgical procedure for thyroid cancer patients. Because we found that cLE increases the phosphorylation level of the MAPK pathway in the brain and the activation of the MAPK pathway is closely related to cell proliferation, this prompted us to consider whether cLE also activates the MAPK pathway in the thyroid and whether it increases the proliferation activity of thyroid cells. This is crucial for the prognosis of a large number of thyroid cancer patients. Therefore, we examined changes in the levels of the Ki67 protein and MAPK pathway phosphorylation in the thyroid (Figure 4A). Interestingly, there was no significant change in thyroid Ki67 after cLE ($p = 0.5551$, Figure 4B), but the phosphorylation levels of MEK1/2 and Erk1/2 significantly decreased after cLE (MEK1/2: $p = 0.0456$; Erk1/2: $p = 0.0340$, Figure 4C,D), and the phosphorylation level of p38 also decreased ($p = 0.0131$, Figure 4E), which is the opposite of the changes in the MAPK pathway in the brain. Additionally, the Ki67 staining results of the thyroid also showed (Figure S3 in supporting information) that there was no significant difference in the proportion of Ki67+ cells in the thyroid between the cLE group and the sham group ($p = 0.4280$, $n = 4$ per group, Figure S3).

The results indicate that, in contrast to the activation of pathways in the brain, cLE may not stimulate the proliferation of thyroid cells. This finding is consolatory for patients with thyroid cancer, at least for the thyroid.

3.5 | Long-term cLE increases p-tau accumulation

The Aβ precursor protein (APP) and its cleavage product, Aβ, are critical markers of AD. cLE not only directly impairs the drainage pathways of the brain's meningeal lymphatic system,[20] but we found that it also affects autophagy. This impairment hinders the clearance of brain wastes, raising the question of whether it leads to AD-like pathological changes. Therefore, we analyzed the alterations in Aβ and p-tau levels after cLE treatment using western blotting (Figure 5A). The results indicated that, while chronic cLE did not result in the accumulation of APP and Aβ1-42 in the brain (APP: $p = 0.5942$; Aβ1-42: $p = 0.3035$; Figure 5B,C), it did lead to p-tau accumulation. The phosphorylation levels of p-tau at different amino acid sites varied after cLE treatment. Notably, phosphorylation at T205, T217, and S396 significantly increased, whereas the levels at S262 and S404 showed a non-significant increase (T205: $p = 0.0048$; T217: $p = 0.0134$; S262: $p = 0.0892$; S396: $p = 0.0058$; S404: $p = 0.1863$; Figure 5D-H).

P-tau (T205) was detected by immunofluorescence staining in the cerebral cortex, hippocampal CA1, hippocampal DG, and thalamus (Figure 6A). Interestingly, p-tau205 increased in various brain regions

pathway enrichment analysis of the eight overlapping genes, primarily related to circadian rhythm ($p < 0.05$). E, Representative western blotting bands depicting *Per2*, *Npas2*, and *Pomc* expression levels in brain tissues from the sham and cLE groups. F–H, Western blotting quantification of *Per2*, *Npas2*, and *Pomc* expression (*Per2*: $p = 0.0135$; *Npas2*: $p = 0.2303$; *Pomc*: $p < 0.0001$; sham: $n = 6$ mice, cLE: $n = 5$ mice). I and J, Representative NeuN and *Pomc* immunofluorescence co-localization images showing *Pomc* expression in neurons within the cortex, hippocampal CA1 region, and hippocampal dentate gyrus (DG) region of the sham and cLE groups (red: NeuN, green: *Pomc*; 40× images on the left panel, with white dashed boxes indicating magnified regions, and 200× magnified images on the right panel). K, Correlation analysis of immunofluorescence co-localization in the cortex, hippocampal CA1 region, hippocampal DG region, and thalamus (cortex: $p = 0.5404$; CA1: $p = 0.0066$; DG: $p = 0.0145$; thalamus: $p = 0.0282$; $n = 5$ mice per group, three slices per mouse, three fields of view per slice). L, Representative sleep electroencephalogram (EEG) energy spectral density plots, EEG waveforms, and bar charts showing the proportions of alpha, beta, theta, and delta wave energy in the two groups of mice (blue line: sham, purple line: cLE). M, Proportions of alpha, beta, theta, and delta wave energy relative to the total energy in the two groups (alpha: $p = 0.0061$; beta: $p = 0.2310$; theta: $p = 0.0043$; delta: $p = 0.0041$; $n = 5$ mice per group). N, Schematic diagram of the hypothesis model. Long-term cLE impairs the sleep cycle entering the non–rapid eye movement (NREM) stage 3, thereby inducing depression-like behaviors.

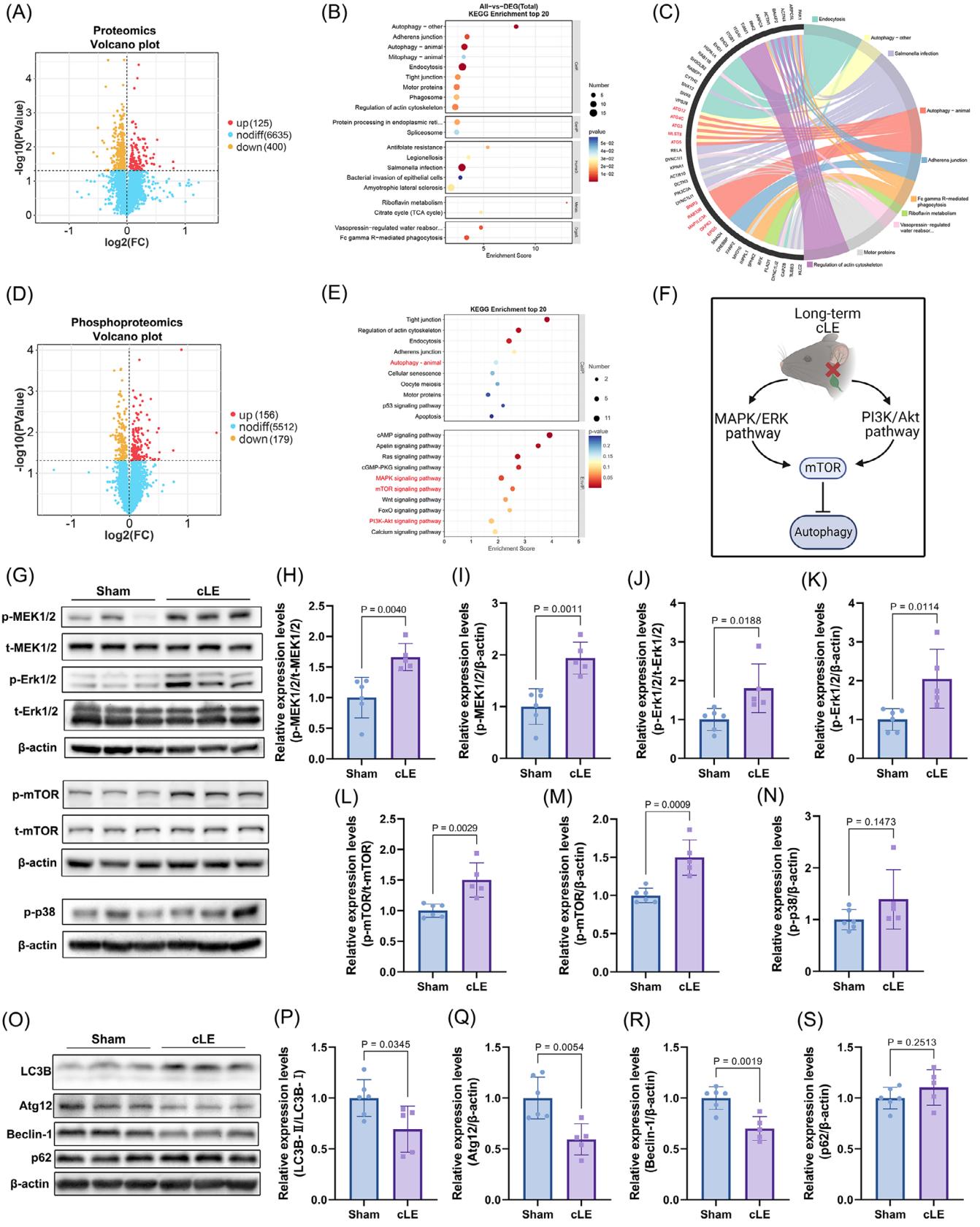

FIGURE 3 Proteomics combined with phosphoproteomics indicates that cervical lymphadenectomy (cLE) activates the mitogen-activated protein kinase (MAPK) pathway in the brain and inhibits autophagy. A, The volcano plot illustrates the upregulated and downregulated differentially expressed proteins in brain proteomics results after cLE ($p < 0.05$, $n = 4$ mice per group). B, The Kyoto Encyclopedia of Genes and Genomes (KEGG) functional enrichment bubble plot of differentially expressed proteins with autophagy-related functions is highlighted in red. C,

after cLE treatment, with statistically significant increases observed in the cortex, CA1, and thalamus (cortex: $p = 0.0004$; CA1: $p = 0.0066$; DG: $p = 0.0664$; thalamus: $p = 0.0315$; Figure 6B-E). Neurofibrillary tangles (NFTs) are a pathological hallmark of AD due to tau hyperphosphorylation. We found NFT-like microstructures by TEM in the brains of cLE group mice (Figure S4 in supporting information). These results suggest that cLE may accelerate the progression of AD-like tauopathy.

3.6 | cLE impaired drainage of brain wastes in mice and humans

We have found an increase in p-tau in brain tissue, so how do brain waste and also AD markers change in peripheral blood after cLE damage drainage? We collected peripheral blood specimens from mice and humans after cLE in acute and chronic phases to examine changes in Aβ and p-tau levels. Mice subjected to cLE exhibited significantly lower levels of Aβ1-42 and p-tau396 in peripheral blood compared to the sham-operated group at both 3 days and 6 months postoperatively (Aβ1-42 3 days: $p = 0.0072$; Aβ1-42 6 months: $p = 0.0275$; p-tau396 3 days: $p = 0.0131$; p-tau396 6 months: $p = 0.0179$; Figure 7A,B). There were no significant differences in plasma Aβ and p-tau396 levels between the pre-operation group and the 3 day sham group (Aβ1-42: $p = 0.3249$; p-tau396: $p = 0.6415$; Figure 7A,B). Additionally, we conducted multifactorial correlation analyses on brain LC3B (LC3B-II/LC3B-I), brain Pomc, brain p-Erk1/2, brain p-tau205, plasma Aβ1-42, and plasma p-tau396 levels, along with results from the EPT, TST, and EEG monitoring in all mice (Figure 7C). The results suggested that elevated p-tau205 and p-Erk1/2, decreased Pomc, and autophagy in the brain were associated with sleep EEG disturbances and anxiety- and depression-like behavior. In contrast, the levels of p-tau396 in peripheral blood and p-Erk1/2 in brain tissue presented an opposite pattern (Figure 7C).

Similarly, we collected preoperative, 3 days postoperative, and 6 months postoperative peripheral blood samples and assessed sleep and mental health scores from seven patients who underwent bilateral cervical lymph node dissection (Table S1 in supporting information). The pattern in human patients at 3 days postoperatively mirrored that in mice, showing a decrease in plasma Aβ1-42 and p-tau396 compared to preoperative levels (Figure 7D,E; Aβ1-42 3 days vs. pre: $p = 0.0273$; p-tau396 3 days vs. pre: $p = 0.0721$). Surprisingly, plasma Aβ1-42 and p-tau396 levels increased at 6 months postoperatively (Figure 7D,E; Aβ1-42 6 months vs. 3 days: $p = 0.0297$; p-tau396 6 months vs. 3 days: $p = 0.0427$), even exceeding preoperative levels in some patients, albeit without statistical significance. However, there was no significant change in sleep, anxiety, or depression status between preoperative and 6 month postoperative patients (Figure 7F,G; PSQI: $p = 0.8291$; HADS: $p = 0.2481$), but it is undoubtedly good news for the patients. Nevertheless, patients' plasma Aβ1-42 and p-tau396 levels were posi-

The chord diagram shows specific differential proteins in the top 10 KEGG functions with the smallest *p* values, with autophagy-related proteins highlighted in red. D, The volcano plot illustrates upregulated and downregulated differentially phosphorylated protein sites in brain phosphoproteomics results after cLE ($p < 0.05$, $n = 4$ mice per group). E, The KEGG functional enrichment bubble plot of differentially phosphorylated proteins with autophagy-regulating pathways is highlighted in red. F, The results of proteomics and phosphoproteomics suggest that long-term cLE activates the MAPK/ extracellular signal-regulated kinase (Erk) pathway and the PI3K pathway, thereby inhibiting autophagy. G, Representative western blot bands show the phosphorylation levels of the Erk1/2 and mechanistic target of rapamycin (mTOR) pathway and p38 in the brain tissues of the two groups of mice. H–N, Bar charts display the phosphorylation level changes of MEK1/2, Erk1/2, mTOR, and p38 (p-MEK1/2[t-MEK1/2]: $p = 0.0040$; p-MEK1/2[β-actin]: $p = 0.0011$; p-Erk1/2[β-actin]: $p = 0.0114$; p-Erk1/2[t-Erk1/2]: $p = 0.0188$; p-mTOR[t-mTOR]: $p = 0.0029$; p-mTOR[β-actin]: $p = 0.0009$; p-p38: $p = 0.1473$; sham: $n = 6$ mice, cLE: $n = 5$ mice). O, Representative western blot bands show the expression of autophagy-related proteins (LC3B, Atg12, Beclin-1, and p62) in the brain tissues of the two groups of mice. P–S, Bar charts display the levels of LC3B-II/LC3B-I, Atg12, Beclin-1, and p62 (LC3B-II/LC3B-I: $p = 0.0345$; Atg12: $p = 0.0054$; Beclin-1: $p = 0.0019$; p62: $p = 0.2513$; sham: $n = 6$ mice, cLE: $n = 5$ mice).

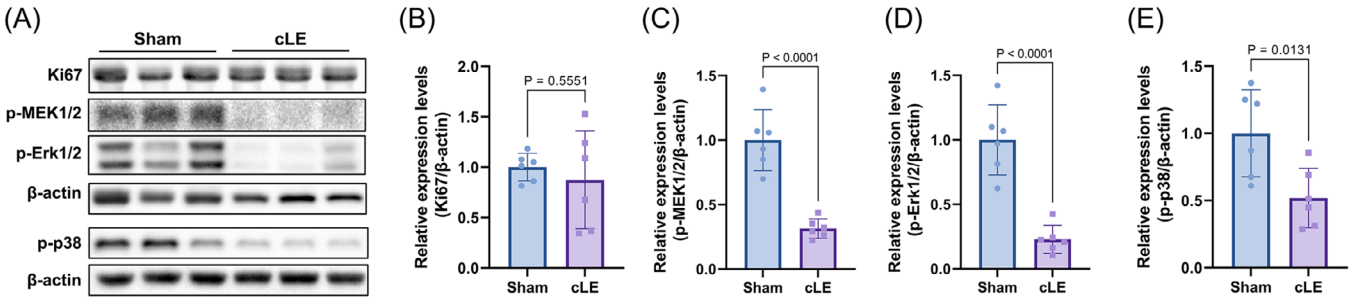

FIGURE 4 Long-term cervical lymphadenectomy (cLE) reduces the phosphorylation levels of the mitogen-activated protein kinase (MAPK) pathway in the thyroid without affecting cell proliferation. A, Representative western blot bands show the Ki67 protein levels and the phosphorylation levels of the MAPK pathway in the thyroid tissues of the two groups of mice. B–E, Bar charts display the Ki67 protein levels and the phosphorylation levels of MEK1/2, extracellular signal-regulated kinase (Erk)1/2, and p38 in the thyroid (Ki67: $p = 0.5551$; p-MEK1/2: $p = 0.0456$; p-Erk1/2: $p = 0.0340$; p-p38: $p = 0.0131$; sham: $n = 6$ mice, cLE: $n = 6$ mice)

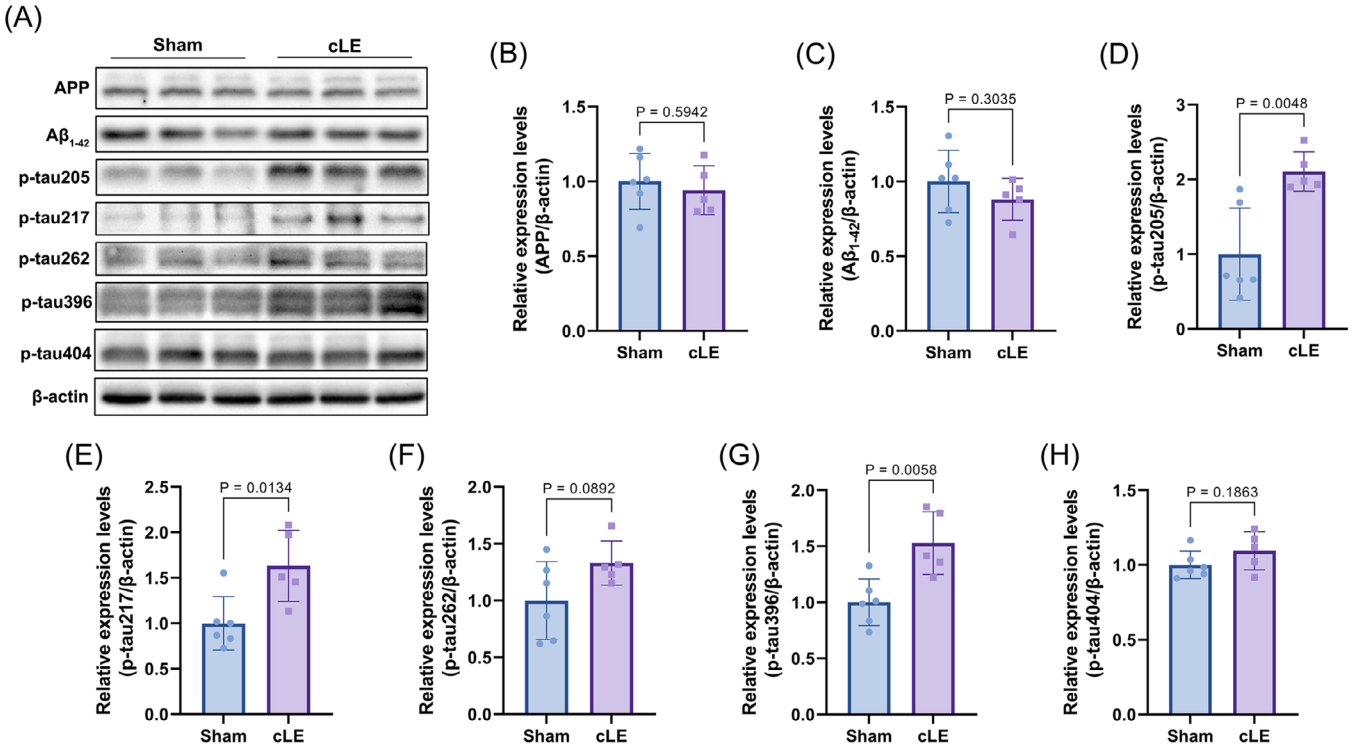

FIGURE 5 Long-term cervical lymphadenectomy (cLE) leads to the accumulation of phosphorylated tau (p-tau) in the brain. A,) Representative western blotting bands show the protein expression levels of amyloid beta (Aβ) precursor protein (APP) and Aβ1-42, as well as the phosphorylation levels of tau at different sites (p-tau205, p-tau217, p-tau262, p-tau396, and p-tau404) in the brains of the two groups of mice. B and C, Bar charts display the protein expression levels of APP and Aβ1-42 in the brain (APP: $p = 0.5942$; Aβ1-42: $p = 0.3035$; sham: $n = 6$ mice, cLE: $n = 5$ mice). D–H, Bar charts show the phosphorylation levels of p-tau205, p-tau217, p-tau262, p-tau396, and p-tau404 in the brain (p-tau205: $p = 0.0048$; p-tau217: $p = 0.0134$; p-tau262: $p = 0.0892$; p-tau396: $p = 0.0058$; p-tau404: $p = 0.1863$; sham: $n = 6$ mice, cLE: $n = 5$ mice)

tively correlated with PSQI and HADS scores (Figure 7H), although not statistically significantly.

4 | DISCUSSION

The findings of this study provide the first evidence that long-term cLE has significant and previously unrecognized effects on neurological health, particularly concerning AD-like pathology. AD is a continuum, with AD pathology occurring years before the onset of mild cognitive impairment, making biomarkers particularly important for early diagnosis.[5] Our results suggest that cLE could contribute to the development of early AD processes (Figure 8, Graphical Abstract), which has profound implications for the millions of individuals who undergo cLE operations annually.

One of the most striking outcomes of this study is the observed increase in p-tau accumulation in the brain after long-term cLE. These pathological hallmarks are characteristic of AD and suggest a potential mechanistic link between cLE and AD-like neurodegeneration. We found that long-term cLE increased phosphorylation at specific sites of tau protein in the brain, such as T205, T217, and S396. Plasma p-tau217 levels have recently emerged as a new biomarker for supporting the diagnosis of AD,[29,30] with p-tau217 being highly specific for detecting amyloid pathology and potentially rising 20 years before cognitive impairment appears.[31]

In contrast, p-tau205 increases after amyloid pathology is present and continues to rise with the clinical progression of AD.[31,32] Studies based on human brain samples suggest that S396 phosphorylation is an early event in AD.[33] Our p-tau205 immunofluorescence, a marker of early pretangles,[34] results revealed tau hyperphosphorylation after cLE. The incidence of AD is closely related to age, with very few cases diagnosed before the age of 50, but affecting more than half of the population by the age of 90.[35] It is generally accepted that mice older than 18 months are considered aged mice,[36,37] while in our study, mice ≈ 8 months old, 6 months post-cLE, exhibited significant early pathological features of AD.

In addition to biomarkers, we also observed AD-like behavioral changes after cLE, including mild cognitive impairment, sleep disturbances, and mental disorders.[38] Cognitive dysfunction is the primary symptom used for diagnosing AD, frequently evaluated in mice using the MWM test.[39,40] Additionally, psychiatric and sleep disorders are recognized as risk factors and prodromal indicators of AD.[41] A large-scale agnostic study, which included 20,214 AD patients from the United Kingdom and 19,458 from France, indicated that depression and anxiety are the initial health conditions associated with AD, occurring at least 9 years before the clinical diagnosis of AD.[7] In humans,

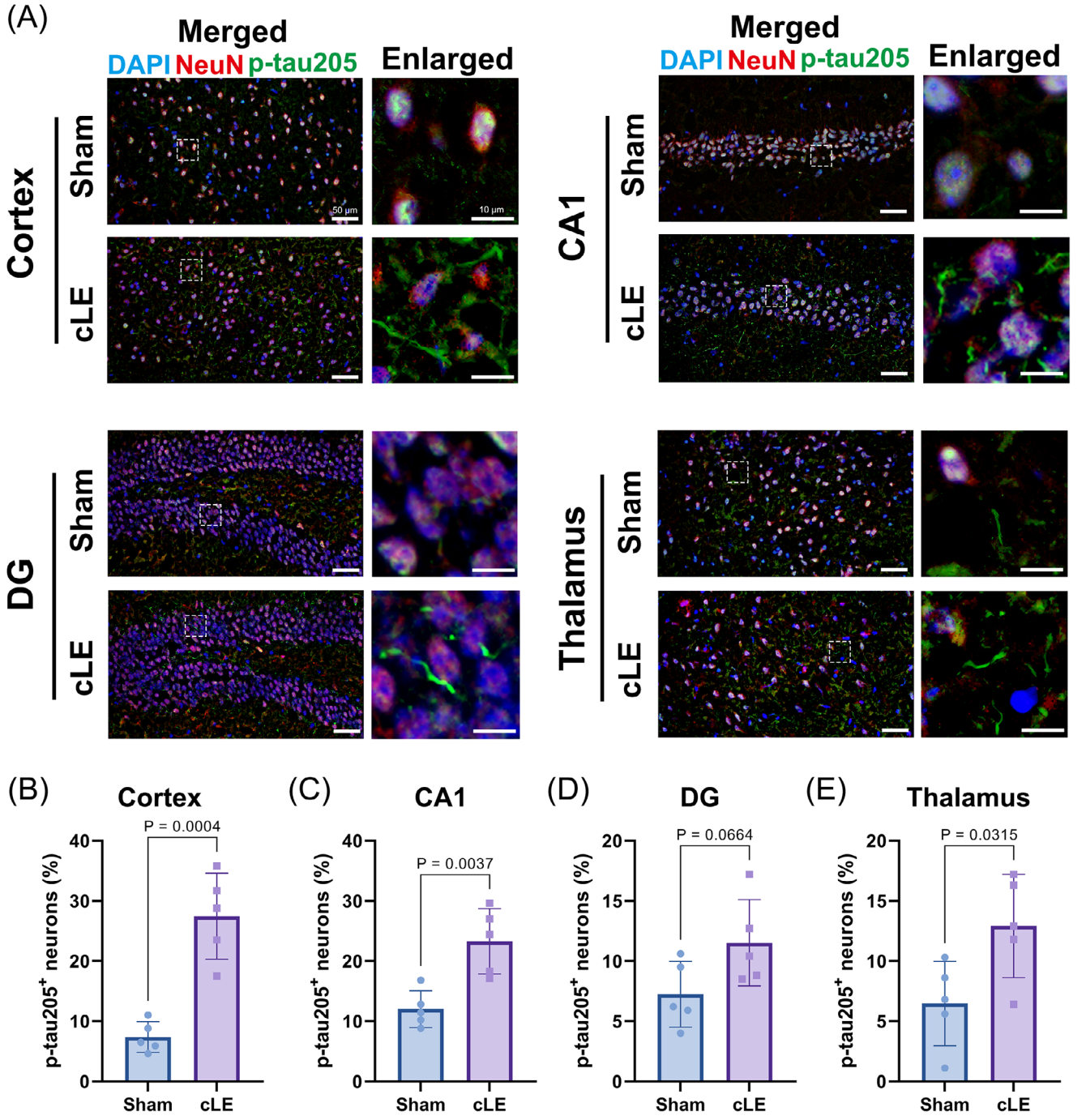

FIGURE 6 Long-term cervical lymphadenectomy (cLE) increases tau phosphorylation levels. A, Representative images of NeuN and phosphorylated tau (p-tau)205 immunofluorescence co-localization in the cerebral cortex, hippocampal CA1 region, hippocampal dentate gyrus (DG) region, and thalamus of the two groups of mice (blue: DAPI, red: NeuN, green: p-tau205; the white dashed boxes are magnified 4×). B–E, The proportion of neurons containing p-tau205 in the cerebral cortex, hippocampal CA1 region, hippocampal DG region, and thalamus (cortex: $p = 0.0004$; CA1: $p = 0.0066$; DG: $p = 0.0664$; thalamus: $p = 0.0315$; $n = 5$ mice per group, three slices per mouse, three fields of view per slice)

NREM stage 1 is the initial phase of sleep, marked by EEG activity similar to quiet wakefulness, characterized by a predominance of alpha and beta waves and a reduction in delta waves. NREM stage 2 is distinguished by spontaneous K-complexes and sleep spindles, while NREM stage 3 features large, slow oscillations with dominant delta waves.[9] Numerous clinical studies have demonstrated a reduction in NREM stage 3 and a prolongation of NREM stage 1 in AD patients.[42–48] Notably, our EEG recordings in cLE mice exhibited increased alpha waves and a significant reduction in delta waves, indicating an increase in NREM stage 1 and a decrease in NREM stage 3, mirroring the sleep patterns commonly observed in clinical AD patients. Tau pathology, sleep disturbances, and psychiatric disorders are recognized as

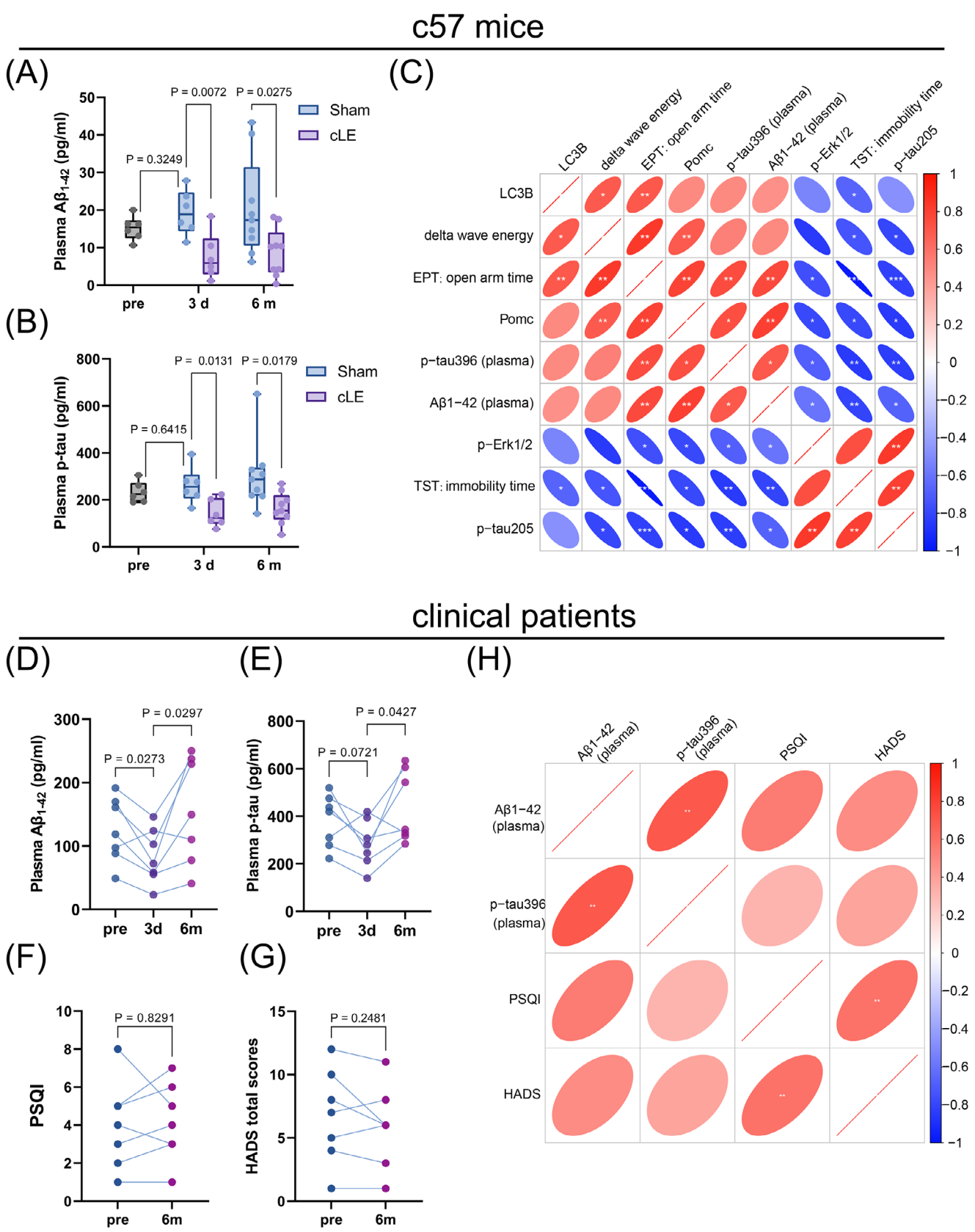

FIGURE 7 Decreased peripheral blood brain waste levels after long-term cervical lymphadenectomy (cLE). A and B, Plasma levels of amyloid beta (Aβ)1-42 and phosphorylated tau (p-tau)396 in the pre-operation group, sham, and cLE groups at 3 days and 6 months after the operation. C, Correlation heat map of brain LC3B (LC3B-II/LC3B-I), brain Pomc, brain p-Erk1/2, brain p-tau205, plasma Aβ1-42, and plasma p-tau396 levels, along with results from the elevated plus-maze test (EPT), tail suspension test (TST), and electroencephalogram (EEG) monitoring. Red represents

early features of AD that precede cognitive decline. Recent research suggests that sleep disturbances are primarily driven by tau pathology, in contrast to the traditional view that attributes them to Aβ accumulation.[49] During AD progression, tau pathology emerges earlier than Aβ plaques in brain regions associated with wakefulness (the ascending reticular activating system), which correlates with the onset of sleep disturbances.[50–52]

Furthermore, sleep disturbances are also a hallmark of pure tauopathy, progressive supranuclear palsy, which is not related to Aβ plaques.[53] This evidence indicates that abnormal tau is the main contributor to early sleep disturbances in AD, while the combined effects of Aβ and tau contribute to more severe sleep disturbances in later stages.[54] Similarly, a recent study suggests that hyperphosphorylation of tau contributes to circadian rhythm dysfunction.[55] These findings align with our observations in cLE mice, which exhibit pronounced tau pathology; neuroelectrophysiological and molecular level analyses indicate sleep disturbances and circadian rhythm dysfunction, accompanied by only mild cognitive impairment and no Aβ burden.

The patients included in this study who underwent clinical cervical lymph node dissection did not exhibit significant sleep disturbances or mood disorders. Interestingly, during the peer review, a Taiwan team led by Chao provided clinical evidence that cervical lymph node dissection increases the risk of dementia.[56] This study retrospectively analyzed 251 patients over 15 years and found that cervical lymph

positive correlation, and blue represents negative correlation. $^{*}p < 0.05$, $^{**}p < 0.01$, $^{***}p < 0.001$. D and E, Plasma levels of Aβ1-42 and p-tau396 in clinical patients at 3 days and 6 months after the surgery. F and G, Pittsburgh Sleep Quality Index (PSQI) and Hospital Anxiety and Depression Scale (HADS) results of clinical patients preoperation and postoperation. H, Correlation heat map of plasma Aβ1-42, plasma p-tau396, PSQI, and HADS total scores. Red represents positive correlation, and blue represents negative correlation. $^{*}p < 0.05$, $^{**}p < 0.01$, $^{***}p < 0.001$.

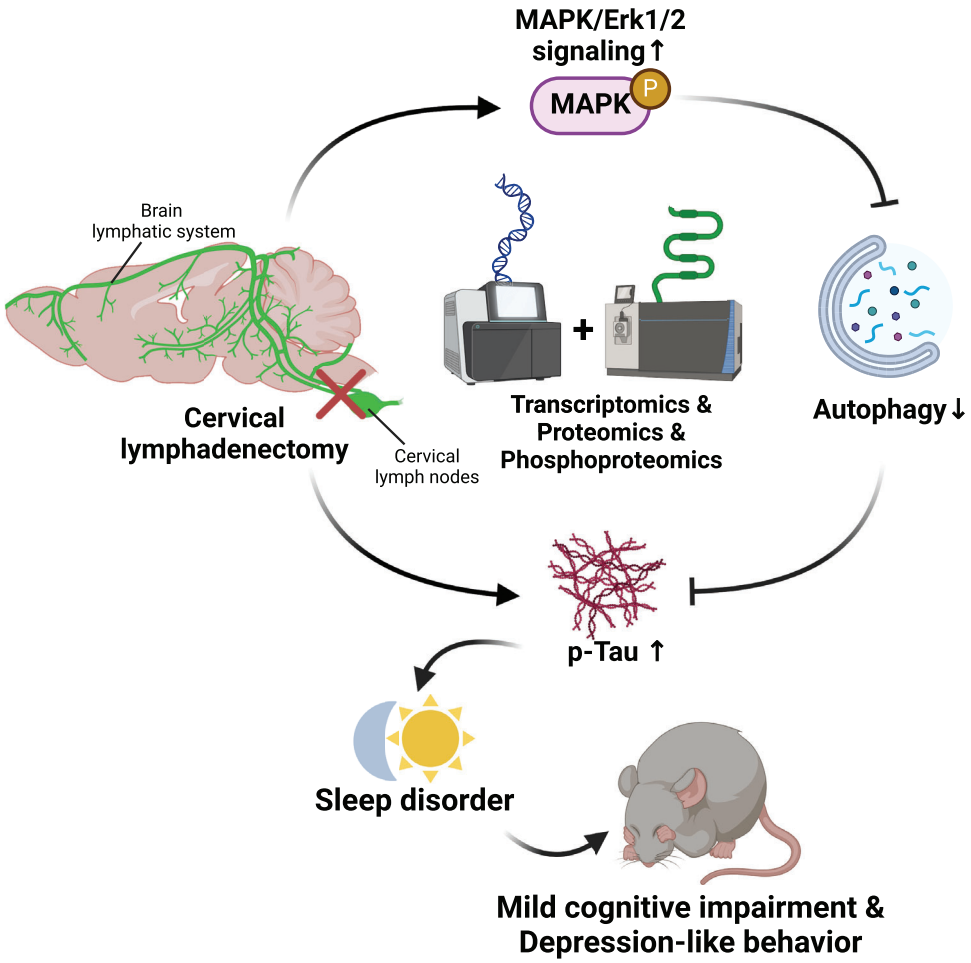

FIGURE 8 Figure abstract of the study. After long-term cervical lymphadenectomy (cLE), there was not only direct disruption of the outward drainage of brain waste products, such as phosphorylated tau (p-tau) and amyloid beta (Aβ) but also activation of cerebral extracellular signal-regulated kinase (Erk)1/2 signaling and impaired autophagy, as revealed by multi-omics analysis. These disruptions led to the accumulation of p-tau. Behaviorally, cLE induced mild cognitive impairment, as well as sleep and mental disorders. This study provides novel evidence of Alzheimer's disease–like tauopathy associated with cLE. MAPK, mitogen-activated protein kinase

node dissection increased the risk of dementia, with bilateral dissection presenting a higher risk than unilateral dissection. This strongly supports our conclusions and suggests that the long-term effects of cLE may require longer follow-up times and the inclusion of more patients.

Cervical lymph nodes serve as a vital conduit between the brain's lymphatic drainage system and the extracranial space.[57–59] Obstruction of this drainage can worsen neurodegenerative diseases such as AD and Parkinson's disease.[60,61] Additionally, brain lymphatic drainage plays a role in hematoma clearance in hemorrhagic brain diseases.[62,63] While brain lymphatic system blockage is rare in clinical settings, cervical lymph node dissection is a standard surgical procedure. Beyond the physical obstruction of the brain lymphatic system's external drainage, the potential effects of cLE on other brain self-cleaning mechanisms remain unclear. Before identifying the brain lymphatic system, it was widely assumed that brain waste was eliminated through endogenous processes like phagocytosis and autophagy.[64] Notably, our multi-omics studies revealed that cLE also impairs the brain's autophagy function. Autophagy impairment is an early feature of AD,[65] and the autophagic activity of microglia and astrocytes is essential for Aβ clearance.[66,67]

Furthermore, Erk1/2 signaling pathway activation not only inhibits autophagy but also suppresses mitophagy.[68,69] Our study is the first to demonstrate that cLE not only blocks the brain lymphatic system but also triggers Erk1/2 signaling, leading to impaired autophagy. Proteomics findings also indicate that cellular endocytic functions are affected, warranting further investigation.

Most studies consider the brain lymphatic system as a physical drainage pathway for the clearance of brain waste. After cLE, impaired lymphatic drainage leads to neuroinflammation and activation of the MAPK pathway.[70] On the other hand, the immune function of the lymphatic system, especially the cervical lymph nodes, cannot be ignored. Recent discoveries emphasize the role of the brain lymphatic system in maintaining immune homeostasis in the central nervous system.[71,72] Antigen-presenting cells carrying brain antigens travel via the brain lymphatic system to the deep cervical lymph nodes to activate T cells.[73] Recent research suggests that CD8+ T cells infiltrating the brain are protective in AD, rather than being culprits.[74,75] cLE blocks the presentation of brain antigens, potentially inhibiting adaptive immunity and promoting AD progression. Based on related literature,[76] we performed a correlation analysis between the proteomics and transcriptomics data. Because the proteomics and transcriptomics data were derived from different batches of animals, the correlation coefficient was low at 0.2486 (Figure S5A in supporting information). We performed functional enrichment analysis on genes/proteins that were differentially expressed in both the transcriptome and proteome (|log2FoldChange > 0.2|), and most of the results were related to the immune system (Figure S5B). This has inspired our next research direction: how cLE affects adaptive immune cells in the brain and promotes neurodegenerative diseases.

We complementarily analyzed all differentially expressed genes in the transcriptome data. Interestingly, KEGG analysis still highlighted circadian rhythm-related functional enrichment and also pointed to neurodegenerative diseases like Parkinson's disease. GO Biological Process (GOBP) primarily indicated immune system–related enrichments and both KEGG and GOBP were related to endoplasmic reticulum pathways (Figure S6A,B in supporting information). Protein misfolding and endoplasmic reticulum stress are common in AD cell pathology,[77] suggesting that cLE may disrupt the function of the endoplasmic reticulum, potentially leading to neurodegenerative disease.

The MAPK pathway in the thyroid does not become activated after cLE, which is different from the brain. We hypothesize that this is because the metabolism and immunity of the thyroid are related to the peripheral circulatory system, which differs from the brain, which has a blood–brain barrier.

In recent years, promoting brain lymphatic drainage has emerged as a prominent focus in the treatment of neurodegenerative diseases, offering a novel therapeutic strategy for AD.[78–80] Our research provides an alternative perspective on the crucial role of cervical lymph in preventing AD pathology. Human patients who underwent bilateral cervical lymph node dissection, in the acute phase (3 days post-operation), exhibited reduced brain waste levels in peripheral blood. This reduction was associated with worsened sleep quality and mental health scores, consistent with findings in animal models. Interestingly, current reports support that surgery or anesthesia elevates[81–84] or does not alter[85,86] Aβ and p-tau in plasma and cerebrospinal fluid, contrary to our findings. This discrepancy may be due to the limited inclusion of otolaryngology and thyroid surgeries in these studies,[85,86] which preserved cervical lymphatic drainage. Plasma Aβ1-42 and p-tau are widely used as early diagnostic markers for AD; however, for patients with impaired brain lymphatic drainage, the levels of brain waste in peripheral blood might not positively correlate with brain levels. Interestingly, the patient's plasma brain waste levels were instead elevated in the chronic phase (6 months post-operation). In fact, bilateral cervical lymph node dissection does not remove all cervical lymph nodes. We hypothesize that this is related to residual other outward drainage pathways of brain waste in humans and AD-like pathology resulting from partial impairment of brain lymphatic drainage. Given our relatively small clinical sample size, larger scale, multicenter prospective studies are needed to confirm and expand upon these findings.

In conclusion, this study is the first to identify AD-like pathology after long-term cervical lymph node dissection and to establish a link between this pathology, Erk1/2 signaling activation, and autophagy suppression, providing critical new insights for AD prevention and treatment. More importantly, the study highlights the necessity for further evaluation of the neurological impacts of cervical lymph node dissection, a procedure that affects millions of people annually.

ACKNOWLEDGMENTS

We thank the Shanghai Luming Biological Technology Co., LTD (Shanghai, China) for providing proteomics and phosphoproteomics technical support. Thanks to BioRender.com for the schematic materials. We thank the Department of General Surgery of Tianjin Medical University General Hospital for supporting the clinical data. This work was supported by the National Natural Science Foundation of China (82071390, 82271394, 82071402, 82171359, 82001323, and

82101434) and Tianjin Key Medical Discipline (Specialty) Construction Project.

CONFLICT OF INTEREST STATEMENT

No potential conflict of interest was reported by the authors. Author disclosures are available in the supporting information.

CONSENT STATEMENT

The clinical ethics committee of the Tianjin Medical University General Hospital approved the clinical trials in this study (approval number: IRB2024-YX-429-01). All patients included in the study signed a consent form. This observational clinical study was registered at the Chinese Clinical Trial Registry (ChiCTR).

ORCID

Chenrui Wu https://orcid.org/0000-0002-4933-6918
Rongcai Jiang https://orcid.org/0000-0002-9119-0115

REFERENCES

1. Obermannová R, Alsina M, Cervantes A, et al. Oesophageal cancer: ESMO Clinical Practice Guideline for diagnosis, treatment and follow-up. *Ann Oncol*. 2022;33(10):992-1004.
2. Machiels JP, René Leemans C, Golusinski W, et al. Squamous cell carcinoma of the oral cavity, larynx, oropharynx and hypopharynx: EHNS-ESMO-ESTRO Clinical Practice Guidelines for diagnosis, treatment and follow-up. *Ann Oncol*. 2020;31(11):1462-1475.
3. Filetti S, Durante C, Hartl D, et al. Thyroid cancer: ESMO Clinical Practice Guidelines for diagnosis, treatment and follow-up†. *Ann Oncol*. 2019;30(12):1856-1883.
4. Bray F, Laversanne M, Sung H, et al. Global cancer statistics 2022: GLOBOCAN estimates of incidence and mortality worldwide for 36 cancers in 185 countries. *CA Cancer J Clin*. 2024;74(3):229-263.
5. Scheltens P, De Strooper B, Kivipelto M, et al. Alzheimer's disease. *Lancet*. 2021;397(10284):1577-1590.
6. Liu Y, Xiao X, Yang Y, et al. The risk of Alzheimer's disease and cognitive impairment characteristics in eight mental disorders: a UK Biobank observational study and Mendelian randomization analysis. *Alzheimers Dement*. 2024;20(7):4841-4853.
7. Nedelec T, Couvy-Duchesne B, Monnet F, et al. Identifying health conditions associated with Alzheimer's disease up to 15 years before diagnosis: an agnostic study of French and British health records. *Lancet Digit Health*. 2022;4(3):e169-e178.
8. Irwin MR, Vitiello MV. Implications of sleep disturbance and inflammation for Alzheimer's disease dementia. *Lancet Neurol*. 2019;18(3):296-306.
9. Slutsky I. Linking activity dyshomeostasis and sleep disturbances in Alzheimer disease. *Nat Rev Neurosci*. 2024;25(4):272-284.
10. Lydiatt WM, Moran J, Burke WJ. A review of depression in the head and neck cancer patient. *Clin Adv Hematol Oncol*. 2009;7(6):397-403.
11. Reich M. [Depression in oncology]. *Cancer Radiother*. 2010;14(6-7):535-538.
12. Howren MB, Christensen AJ, Pagedar NA. Prevalence and persistence of depressive symptoms during the first year postdiagnosis in a large sample of patients with head and neck cancer. *Am J Otolaryngol*. 2024;45(3):104257.
13. Li N, Otomaru T, Taniguchi H. Sleep quality in long-term survivors of head and neck cancer: preliminary findings. *Support Care Cancer*. 2017;25(12):3741-3748.
14. Louveau A, Smirnov I, Keyes TJ, et al. Structural and functional features of central nervous system lymphatic vessels. *Nature*. 2015;523(7560):337-341.
15. Xie L, Kang H, Xu Q, et al. Sleep drives metabolite clearance from the adult brain. *Science*. 2013;342(6156):373-377.
16. Da Mesquita S, Louveau A, Vaccari A, et al. Functional aspects of meningeal lymphatics in ageing and Alzheimer's disease. *Nature*. 2018;560(7717):185-191.
17. Formolo DA, Yu J, Lin K, et al. Leveraging the glymphatic and meningeal lymphatic systems as therapeutic strategies in Alzheimer's disease: an updated overview of nonpharmacological therapies. *Mol Neurodegener*. 2023;18(1):26.
18. Sweeney MD, Zlokovic BV. A lymphatic waste-disposal system implicated in Alzheimer's disease. *Nature*. 2018;560(7717):172-174.
19. Tarasoff-Conway JM, Carare RO, Osorio RS, et al. Clearance systems in the brain-implications for Alzheimer disease. *Nat Rev Neurol*. 2015;11(8):457-470.
20. Wang L, Zhang Y, Zhao Y, Marshall C, Wu T, Xiao M. Deep cervical lymph node ligation aggravates AD-like pathology of APP/PS1 mice. *Brain Pathol*. 2019;29(2):176-192.
21. Shao L, Mori S, Yagishita Y, et al. Lymphatic mapping of mice with systemic lymphoproliferative disorder: usefulness as an inter-lymph node metastasis model of cancer. *J Immunol Methods*. 2013;389(1-2):69-78.
22. Van den Broeck W, Derore A, Simoens P. Anatomy and nomenclature of murine lymph nodes: descriptive study and nomenclatory standardization in BALB/cAnNCrl mice. *J Immunol Methods*. 2006;312(1-2):12-19.
23. Love MI, Huber W, Anders S. Moderated estimation of fold change and dispersion for RNA-seq data with DESeq2. *Genome Biol*. 2014;15(12):550.
24. Cheng A, Grant CE, Noble WS, Bailey TL. MoMo: discovery of statistically significant post-translational modification motifs. *Bioinformatics*. 2019;35(16):2774-2782.
25. Wu C, Du M, Yu R, et al. A novel mechanism linking ferroptosis and endoplasmic reticulum stress via the circPtpn14/miR-351-5p/5-LOX signaling in melatonin-mediated treatment of traumatic brain injury. *Free Radic Biol Med*. 2022;178:271-294.
26. Piñero J, Ramírez-Anguita JM, Saüch-Pitarch J, et al. The DisGeNET knowledge platform for disease genomics: 2019 update. *Nucleic Acids Res*. 2020;48(D1):D845-D855.
27. Godino-Gimeno A, Leal E, Chivite M, et al. Role of melanocortin system in the locomotor activity rhythms and melatonin secretion as revealed by agouti-signalling protein (asip1) overexpression in zebrafish. *J Pineal Res*. 2024;76(1):e12939.
28. Hedges V. *Introduction to Neuroscience. Michigan State University*; 2022.
29. Barthélemy NR, Saef B, Li Y, et al. CSF tau phosphorylation occupancies at T217 and T205 represent improved biomarkers of amyloid and tau pathology in Alzheimer's disease. *Nat Aging*. 2023;3(4):391-401.
30. Barthélemy NR, Horie K, Sato C, Bateman RJ. Blood plasma phosphorylated-tau isoforms track CNS change in Alzheimer's disease. *J Exp Med*. 2020;217(11):e20200861.
31. Barthélemy NR, Li Y, Joseph-Mathurin N, et al. A soluble phosphorylated tau signature links tau, amyloid and the evolution of stages of dominantly inherited Alzheimer's disease. *Nat Med*. 2020;26(3):398-407.
32. Lantero-Rodriguez J, Montoliu-Gaya L, Benedet AL, et al. CSF p-tau205: a biomarker of tau pathology in Alzheimer's disease. *Acta Neuropathol*. 2024;147(1):12.
33. Mondragón-Rodríguez S, Perry G, Luna-Muñoz J, Acevedo-Aquino MC, Williams S. Phosphorylation of tau protein at sites Ser(396-404) is one of the earliest events in Alzheimer's disease and Down syndrome. *Neuropathol Appl Neurobiol*. 2014;40(2):121-135.
34. Hamlin D, Ryall C, Turner C, Faull R, Murray HC, Curtis MA. Characterization of neurofibrillary tangle immunophenotype signatures

to classify tangle maturity in Alzheimer's disease. *Alzheimers Dement*. 2024;20(7):4803-4817.
35. Alzheimer's Association. 2016 Alzheimer's disease facts and figures. *Alzheimers Dement*. 2016;12(4):459-509.
36. Dutta S, Sengupta P. Men and mice: relating their ages. *Life Sci*. 2016;152:244-248.
37. Wegmann S, Bennett RE, Delorme L, et al. Experimental evidence for the age dependence of tau protein spread in the brain. *Sci Adv*. 2019;5(6):eaaw6404.
38. Livingston G, Huntley J, Sommerlad A, et al. Dementia prevention, intervention, and care: 2020 report of the Lancet Commission. *Lancet*. 2020;396(10248):413-446.
39. Chen G, Chen KS, Knox J, et al. A learning deficit related to age and beta-amyloid plaques in a mouse model of Alzheimer's disease. *Nature*. 2000;408(6815):975-979.
40. Possin KL, Sanchez PE, Anderson-Bergman C, et al. Cross-species translation of the Morris maze for Alzheimer's disease. *J Clin Invest*. 2016;126(2):779-783.
41. Porsteinsson AP, Isaacson RS, Knox S, Sabbagh MN, Rubino I. Diagnosis of early Alzheimer's disease: clinical practice in 2021. *J Prev Alzheimers Dis*. 2021;8(3):371-386.
42. Maestri M, Carnicelli L, Tognoni G, et al. Non-rapid eye movement sleep instability in mild cognitive impairment: a pilot study. *Sleep Med*. 2015;16(9):1139-1145.
43. Liu S, Pan J, Tang K, et al. Sleep spindles, K-complexes, limb movements and sleep stage proportions may be biomarkers for amnestic mild cognitive impairment and Alzheimer's disease. *Sleep Breath*. 2020;24(2):637-651.
44. Bliwise DL, Tinklenberg J, Yesavage JA, et al. REM latency in Alzheimer's disease. *Biol Psychiatry*. 1989;25(3):320-328.
45. Liguori C, Placidi F, Izzi F, Spanetta M, Mercuri NB, Di Pucchio A. Sleep dysregulation, memory impairment, and CSF biomarkers during different levels of neurocognitive functioning in Alzheimer's disease course. *Alzheimers Res Ther*. 2020;12(1):5.
46. Brunetti V, D'Atri A, Della Marca G, et al. Subclinical epileptiform activity during sleep in Alzheimer's disease and mild cognitive impairment. *Clin Neurophysiol*. 2020;131(5):1011-1018.
47. D'Atri A, Scarpelli S, Gorgoni M, et al. EEG alterations during wake and sleep in mild cognitive impairment and Alzheimer's disease. *iScience*. 2021;24(4):102386.
48. Liguori C, Romigi A, Nuccetelli M, et al. Orexinergic system dysregulation, sleep impairment, and cognitive decline in Alzheimer disease. *JAMA Neurol*. 2014;71(12):1498-1505.
49. Lew CH, Petersen C, Neylan TC, Grinberg LT. Tau-driven degeneration of sleep- and wake-regulating neurons in Alzheimer's disease. *Sleep Med Rev*. 2021;60:101541.
50. Ishii T. Distribution of Alzheimer's neurofibrillary changes in the brain stem and hypothalamus of senile dementia. *Acta Neuropathol*. 1966;6(2):181-187.
51. Tomlinson BE, Irving D, Blessed G. Cell loss in the locus coeruleus in senile dementia of Alzheimer type. *J Neurol Sci*. 1981;49(3):419-428.
52. Ehrenberg AJ, Nguy AK, Theofilas P, et al. Quantifying the accretion of hyperphosphorylated tau in the locus coeruleus and dorsal raphe nucleus: the pathological building blocks of early Alzheimer's disease. *Neuropathol Appl Neurobiol*. 2017;43(5):393-408.
53. Walsh CM, Ruoff L, Walker K, et al. Sleepless night and day, the plight of progressive supranuclear palsy. *Sleep*. 2017;40(11):zsx154.
54. Morrone CD, Raghuraman R, Hussaini SA, Yu WH. Proteostasis failure exacerbates neuronal circuit dysfunction and sleep impairments in Alzheimer's disease. *Mol Neurodegener*. 2023;18(1):27.
55. Warfield AE, Gupta P, Ruhmann MM, et al. A brainstem to circadian system circuit links tau pathology to sundowning-related disturbances in an Alzheimer's disease mouse model. *Nat Commun*. 2023;14(1):5027.
56. Chao S, Kuan C, Huang C, et al. Association between cervical lymph node dissection and dementia: a retrospective analysis. *J Plast Reconstr Aesthet Surg*. 2024;99:584-591.
57. Rasmussen MK, Mestre H, Nedergaard M. Fluid transport in the brain. *Physiol Rev*. 2022;102(2):1025-1151.
58. Yankova G, Bogomyakova O, Tulupov A. The glymphatic system and meningeal lymphatics of the brain: new understanding of brain clearance. *Rev Neurosci*. 2021;32(7):693-705.
59. Albayram MS, Smith G, Tufan F, et al. Non-invasive MR imaging of human brain lymphatic networks with connections to cervical lymph nodes. *Nat Commun*. 2022;13(1):203.
60. Ishida K, Yamada K, Nishiyama R, et al. Glymphatic system clears extracellular tau and protects from tau aggregation and neurodegeneration. *J Exp Med*. 2022;219(3):e20211275.
61. Zou W, Pu T, Feng W, et al. Blocking meningeal lymphatic drainage aggravates Parkinson's disease-like pathology in mice overexpressing mutated α-synuclein. *Transl Neurodegener*. 2019;8:7.
62. Yuan J, Liu X, Nie M, et al. Inactivation of ERK1/2 signaling mediates dysfunction of basal meningeal lymphatic vessels in experimental subdural hematoma. *Theranostics*. 2024;14(1):304-323.
63. Chen J, Wang L, Xu H, et al. Meningeal lymphatics clear erythrocytes that arise from subarachnoid hemorrhage. *Nat Commun*. 2020;11(1):3159.
64. Smyth L, Beschorner N, Nedergaard M, Kipnis J. Cellular contributions to glymphatic and lymphatic waste clearance in the brain. *Cold Spring Harb Perspect Biol*. 2024:a041370.
65. Hung C, Livesey FJ. Endolysosome and autophagy dysfunction in Alzheimer disease. *Autophagy*. 2021;17(11):3882-3883.
66. Kim S, Chun H, Kim Y, et al. Astrocytic autophagy plasticity modulates Aβ clearance and cognitive function in Alzheimer's disease. *Mol Neurodegener*. 2024;19(1):55.
67. Choi I, Wang M, Yoo S, et al. Autophagy enables microglia to engage amyloid plaques and prevents microglial senescence. *Nat Cell Biol*. 2023;25(7):963-974.
68. Magrì A, Lipari C, Risiglione P, et al. ERK1/2-dependent TSPO overactivation associates with the loss of mitophagy and mitochondrial respiration in ALS. *Cell Death Dis*. 2023;14(2):122.
69. Cea M, Cagnetta A, Fulciniti M, et al. Targeting NAD+ salvage pathway induces autophagy in multiple myeloma cells via mTORC1 and extracellular signal-regulated kinase (ERK1/2) inhibition. *Blood*. 2012;120(17):3519-3529.
70. Almutary AG, Begum MY, Kyada AK, et al. Inflammatory signaling pathways in Alzheimer's disease: mechanistic insights and possible therapeutic interventions. *Ageing Res Rev*. 2025;104:102548.
71. Castellani G, Croese T, Peralta Ramos JM, Schwartz M. Transforming the understanding of brain immunity. *Science*. 2023;380(6640):eabo7649.
72. Kim MW, Gao W, Lichti CF, et al. Endogenous self-peptides guard immune privilege of the central nervous system. *Nature*. 2025;637(8044):176-183.
73. Louveau A, Herz J, Alme MN, et al. CNS lymphatic drainage and neuroinflammation are regulated by meningeal lymphatic vasculature. *Nat Neurosci*. 2018;21(10):1380-1391.
74. Su W, Saravia J, Risch I, et al. CXCR6 orchestrates brain CD8(+) T cell residency and limits mouse Alzheimer's disease pathology. *Nat Immunol*. 2023;24(10):1735-1747.
75. Reagin KL, Funk KE. CD8(+) T cells pump the brakes on Alzheimer's disease. *Nat Immunol*. 2023;24(10):1597-1598.
76. Li Z, Liu N, Zhang W, et al. Integrated transcriptome and proteome analysis provides insight into chilling-induced dormancy breaking in Chimonanthus praecox. *Hortic Res*. 2020;7(1):198.
77. Lim D, Tapella L, Dematteis G, Genazzani AA, Corazzari M, Verkhratsky A. The endoplasmic reticulum stress and unfolded protein response in Alzheimer's disease: a calcium dyshomeostasis perspective. *Ageing Res Rev*. 2023;87:101914.

78. Du T, Raghunandan A, Mestre H, et al. Restoration of cervical lymphatic vessel function in aging rescues cerebrospinal fluid drainage. *Nat Aging*. 2024;4(10):1418-1431.
79. Nedergaard M, Goldman SA. Glymphatic failure as a final common pathway to dementia. *Science*. 2020;370(6512):50-56.
80. Wang Y, Monai H. Transcranial direct current stimulation alters cerebrospinal fluid-interstitial fluid exchange in mouse brain. *Brain Stimul*. 2024;17(3):620-632.
81. Planel E, Bretteville A, Liu L, et al. Acceleration and persistence of neurofibrillary pathology in a mouse model of tauopathy following anesthesia. *FASEB J*. 2009;23(8):2595-2604.
82. Anckarsäter R, Anckarsäter H, Bromander S, Blennow K, Wass C, Zetterberg H. Non-neurological surgery and cerebrospinal fluid biomarkers for neuronal and astroglial integrity. *J Neural Transm (Vienna)*. 2014;121(6):649-653.
83. Whittington RA, Bretteville A, Dickler MF, Planel E. Anesthesia and tau pathology. *Prog Neuropsychopharmacol Biol Psychiatry*. 2013;47:147-155.
84. Feinstein I, Wilson EN, Swarovski MS, Andreasson KI, Angst MS, Greicius MD. Plasma biomarkers of tau and neurodegeneration during major cardiac and noncardiac surgery. *JAMA Neurol*. 2021;78(11):1407-1409.
85. Reese M, Wong MK, Cheong V, et al. Cognitive and cerebrospinal fluid Alzheimer's disease-related biomarker trajectories in older surgical patients and matched nonsurgical controls. *Anesthesiology*. 2024;140(5):963-978.
86. Berger M, Browndyke JN, Cooter Wright M, et al. Postoperative changes in cognition and cerebrospinal fluid neurodegenerative disease biomarkers. *Ann Clin Transl Neurol*. 2022;9(2):155-170.

SUPPORTING INFORMATION

Additional supporting information can be found online in the Supporting Information section at the end of this article.

How to cite this article: Wu C, Yuan J, Tian Y, et al. Tauopathy after long-term cervical lymphadenectomy. *Alzheimer's Dement*. 2025;21:e70136. https://doi.org/10.1002/alz.70136